Published in final edited form as:
Eur Biophys J. 2012 September ; 41(9): 755–767. doi:10.1007/s00249-012-0850-4.

Effects of the lung surfactant protein B construct Mini-B on lipid bilayer order and topography

Dharamaraju Palleboina,
Department of Physics and Physical Oceanography, Memorial University of Newfoundland, St. John's, NL A1B 3X7, Canada

Alan J. Waring,
Department of Medicine, Geffen School of Medicine, University of California, Los Angeles, CA 90024, USA

Robert H. Notter,
University of Rochester School of Medicine, 601 Elmwood Ave (Box 850), Rochester, NY 14642, USA

Valerie Booth, and
Department of Physics and Physical Oceanography, Memorial University of Newfoundland, St. John's, NL A1B 3X7, Canada

Department of Biochemistry, Memorial University of Newfoundland, St. John's, NL A1B 3X7, Canada

Michael Morrow
Department of Physics and Physical Oceanography, Memorial University of Newfoundland, St. John's, NL A1B 3X7, Canada

Michael Morrow: mmorrow@mun.ca

Abstract

The hydrophobic lung surfactant protein, SP-B, is essential for survival. Cycling of lung volume during respiration requires a surface-active lipid–protein layer at the alveolar air–water interface. SP-B may contribute to surfactant layer maintenance and renewal by facilitating contact and transfer between the surface layer and bilayer reservoirs of surfactant material. However, only small effects of SP-B on phospholipid orientational order in model systems have been reported. In this study, N-terminal ($SP\text{-}B_{8–25}$) and C-terminal ($SP\text{-}B_{63–78}$) helices of SP-B, either linked as Mini-B or unlinked but present in equal amounts, were incorporated into either model phospholipid mixtures or into bovine lipid extract surfactant in the form of vesicle dispersions or mechanically oriented bilayer samples. Deuterium and phosphorus nuclear magnetic resonance (NMR) were used to characterize effects of these peptides on phospholipid chain orientational order, headgroup orientation, and the response of lipid–peptide mixtures to mechanical orientation by mica plates. Only small effects on chain orientational order or headgroup orientation, in either vesicle or mechanically oriented samples, were seen. In mechanically constrained samples, however, Mini-B and its component helices did have specific effects on the propensity of lipid–peptide mixtures to form unoriented bilayer populations which do not exchange with the oriented fraction on the timescale of the NMR experiment. Modification of local bilayer orientation, even in the presence of mechanical constraint, may be relevant to the transfer of material from bilayer

Correspondence to: Michael Morrow, mmorrow@mun.ca.

reservoirs to a flat surface-active layer, a process that likely requires contact facilitated by the formation of highly curved protrusions.

Keywords

Lung surfactant; Pulmonary surfactant; Surfactant protein B (SP-B); Deuterium NMR; Oriented bilayer; Orientational order

Introduction

Changes in lung volume during breathing are enabled by a surfactant layer which reduces surface tension at the air–water interface within the alveoli (Goerke 1998; Pérez-Gil 2002; Zuo et al. 2008; Possmayer et al. 2010). Approximately 90 % of lung surfactant dry weight is accounted for by lipids, particularly phosphatidylcholine and phosphatidylglycerol (Postle et al. 2001; Hildebran et al. 1979; Lang et al. 2005). The remaining dry weight is accounted for by four proteins, of which two, SP-A and SP-D, are large, hydrophilic oligomers that contribute to host defense activity (McCormack 1998; Crouch 1998). The other two proteins, SP-B and SP-C, are small hydrophobic proteins that appear to modify spreading and adsorption of the surface-active film at the air–water interface and which may also be important for maintenance of the film and recruitment of new or recycled material to the film as the area of the air–water interface cycles during respiration (Perez-Gil and Weaver 2010; Possmayer et al. 2010). The transfer of surfactant material from bilayer reservoirs to the surface-active layer presumably requires close contact and fusion between portions of the bilayer surface and the surface layer.

Of the four lung surfactant proteins, only SP-B is known to be essential for lung function (Whitsett et al. 1995; Clark et al. 1995; Nogee et al. 1994). The monomer of this protein contains 79 amino acid residues and carries a charge of +7 at neutral pH (Hawgood et al. 1998). The SP-B monomer comprises at least four amphipathic α-helical segments. In lung surfactant, SP-B exists as a homodimer stabilized by three intramolecular and one intermolecular disulfide bonds. The primary structure of SP-B is shown schematically in Fig. 1a.

A number of SP-B fragments have been synthesized and studied both in animal models and in vitro (Waring et al. 2005; Walther et al. 2002; Revak et al. 1991; Kang et al. 1996; Baatz et al. 1991; Ryan et al. 2005; Serrano et al. 2006). One such fragment, Mini-B, is a concatenation of the N-terminal and C-terminal helices of SP-B, and retains SP-B's overall charge of +7, its amphipathic helical character, and two helix-linking disulfide bonds. Figure 1b shows the primary structure of Mini-B. In surfactant-deficient rats, Mini-B was found to support blood oxygenation levels at least as effectively as full-length SP-B (Waring et al. 2005; Walther et al. 2010). A peptide consisting of SP-B residues 63–78, known as SP-B_{CTERM} or SP-$B_{63–78}$, was found to retain almost half of the full SP-B activity in such studies. Interestingly, SP-$B_{8–25}$ and SP-$B_{63–78}$ are much more active when they are covalently joined inMini-B than when present as individual peptides (Waring et al. 2005). Mini-B has also been combined with a phospholipase-resistant diether phosphonolipid to form a synthetic surfactant with high dynamic surface activity (Walther et al. 2007).

Solution NMR has been used to find high-resolution structures of Mini-B in sodium dodecyl sulfate (SDS) micelles (Sarker et al. 2007), of SP-$B_{63–78}$ in hexafluoropropanol and in SDS micelles (Booth et al. 2004), and of an N-terminal SP-B fragment, SP-$B_{11–25}$, in methanol (Kurutz and Lee 2002). Despite the critical importance of SP-B in breathing, detailed understanding of the functional role played by interactions between SP-B and surfactant

lipids remains elusive. ^{2}H NMR studies of chain-labeled phospholipids in multilamellar vesicle surfactant model systems showed only small perturbations of lipid chain orientational order, and thus lipid area, in the liquid by either SP-B (Dico et al. 1997; Morrow et al. 2007) or the SP-$B_{8–25}$ fragment (Russell-Schulz et al. 2009). However, the extent to which such small perturbations of lipid chain orientational order, as observed in liposomes, might contribute to the unique function of SP-B in lung surfactant remained unclear.

For studies of peptide–lipid interactions, information obtained from mechanically oriented bilayers can usefully complement that obtained from liposome samples. Recent studies of the C-terminal SP-B fragment, SP-$B_{63–78}$, in mechanically oriented bilayers of 1-palmitoyl-2-oleoyl-*sn*-glycero-3-phosphocholine (POPC), 1-palmitoyl-2-oleoyl-*sn*-glycero-3-phospho-(1′-*rac*glycerol) (POPG), POPC/POPG, and bovine lipid extract surfactant (BLES) (Yang et al. 2009; Bertani et al. 2012) showed that, in addition to a small perturbation of lipid chain orientational order, the C-terminal SP-B fragment also induced the formation of unoriented bilayer regions that were large enough to preclude averaging by exchange with the oriented bilayer fraction. While it is known that peptides can interfere with the formation of well-oriented bilayers, it is important to note the possible relevance, for surfactant function, of peptide-induced departures from bilayer planarity or of changes in how bilayers respond to the orienting influence of an adjacent flat surface; For example, rapid adsorption of material from bilayer structures into monolayers is an essential aspect of surfactant function and is likely to require bridging of surfaces by highly curved stalk structures (Zuo et al. 2008; Rugonyi et al. 2008; Possmayer et al. 2010). Maintenance of the surface-active layer is also thought to require that material squeezed out of the monolayer during compression remain anchored to the monolayer and available for recruitment back into the monolayer during expansion. The N-terminal region of SP-B has been implicated in the stabilization of so-called nanosilo reservoirs (Frey et al. 2010), and the formation of such structures presumably involves highly curved intermediate states. Accordingly, a propensity for SP-B and its fragments to compete with the orienting influence of a proximal flat surface, such as in a mechanically oriented bilayer sample, might be relevant to surfactant function.

The study reported here examines lipid bilayer perturbation by the N-terminal and C-terminal helices of SP-B either linked in the form of Mini-B (SP-$B_{8–25}$ plus SP-$B_{63–78}$) or unlinked (SP-$B_{8–25}$ and SP-$B_{63–78}$) but present in equimolar amounts. The effects of these SP-B peptide fragments on lipid chain orientational order and longer length-scale bilayer orientation have been separated by comparing spectra obtained from multilamellar vesicle and from mechanically oriented bilayers. Such comparisons have been carried out for both POPC-d_{31}/POPG model mixtures, to facilitate comparisons with earlier work (e.g., Yang et al. 2009), and for BLES, which is a nearly complete natural surfactant. It is found that, at concentrations low enough for average lipid chain orientational order to be negligibly perturbed by short-range interactions, these peptides can influence bilayer topography over larger length scales and interfere with mechanical bilayer orientation in some mechanically oriented samples. Consideration is given to the possibility that the resulting mosaic spread reflects lipid–peptide interactions that might also be relevant to the promotion of curved or protruding surfaces as implied by some models of surfactant cycling during respiration. Interesting distinctions are found between the effects of Mini-B and a mixture of its unlinked helix components on the model POPC/POPG mixture at 23 °C, which is well above the gel-to-liquid crystal transition temperature for POPC/POPG, and on BLES at 35 °C, which is only a few degrees above the corresponding transition in BLES.

Methods and materials

The phospholipids 1-palmitoyl-d_{31}-2-oleoyl-*sn*-glycero-3-phosphocholine (POPC-d_{31}), 1-palmitoyl-2-oleoyl-*sn*-glycero-3 phospho-(1′-*rac*-glycerol) (POPG), and 1,2-dipalmitoyl-d_{62}-*sn*-glycero-3-phosphocholine (DPPC-d_{62}) were obtained from Avanti Polar Lipids (Alabaster, AL) and used without further purification. Bovine lipid extract surfactant (BLES), a clinically used surfactant, was provided in saline dispersion form, as a donation from BLES Biochemicals (London, Canada). The concentration was determined, by phosphorus assay, to be 22.6 mg/ml. Chloroform ($CHCl_3$) and methanol (MeOH) were obtained from the Fisher Scientific Company (Toronto). Muscovite mica (grade V-4, dimensions 75 mm × 25 mm × 0.26 mm) was purchased from Structure Probe (West Chester, PA).

Mini-B is a disulfide-linked construct of both the N-terminal (8–25) and C-terminal (63–78) portions of SP-B. Its amino acid sequence is shown in Fig. 1b. The peptide was synthesized via solid-phase methods employing *O*-fluorenylmethyl-oxycarbonyl (Fmoc) chemistry as in Sarker et al. (2007). Organic solvents and other reagents used for Mini-B peptide synthesis and purification were of high-performance liquid chromatography (HPLC) grade or better. The peptide was assembled on a prederivatized *N*-Fmoc-*O*-*tert*–butylserine, *p*-hydroxymethylphenoxy (HMP) resin (AnaSpec). Deprotection and cleavage of the peptide from the resin were followed by cold precipitation with *tert*-butyl ether. Crude product was then purified by preparative reversed-phase HPLC with a Vydac C-18 column. The molecular weight of the peptide was confirmed by fast atom bombardment or matrix-assisted laser desorption/ionization time-of-flight (MALDI-TOF) mass spectrometry. Its purity was determined and found to exceed 95 % by analytical HPLC. The peptide was lyophilized and stored in a refrigerator at 4 °C. The N-terminal SP-B peptide (CWLCRALIKRIQAMIPKG, residues 8–25 of SP-B) was prepared in a similar way. The C-terminal segment (GRALPQLVCRLVLRCSM) of Mini-B was expressed as a recombinant protein in *Escherichia coli* and purified via nickel affinity chromatography using the approach described by Lindhout et al. (2003). In this approach, the terminal M is replaced by A to facilitate cyanogen bromide cleavage of the expressed peptide from its fusion protein.

For each of the peptide-containing samples, the total peptide accounted for approximately 5 % of the dry sample mass, corresponding to nominal concentration of approximately 1 mol %. Peptide amounts were determined by weight after multiple dialyzations to remove as much solvent as possible. Measuring peptide weights in a consistent way defines an upper limit on peptide concentration, but because the dry peptide can retain up to 20 % trifluoroacetic acid (TFA) by weight after repeated dialysis, the actual peptide concentration in each sample is expected to be in the range of 0.8–1 mol%.

To prepare mechanically oriented bilayers of POPC-d_{31}/POPG, with or without peptide (1 mol%), specific mixtures of dry components containing approximately 9 mg of total lipid mass were dissolved in 150 μL $CHCl_3$/MeOH (1:1) and then deposited, in roughly 1 μL volumes, at the center of freshly cleaved mica plates cut to dimensions of either 5 mm × 12 mm or 12 mm ×12 mm. The deposited solution was allowed to dry on each plate for 3–5 min after each cycle of deposition. This was repeated until all of the solution was used, after which the mica plates were left in a fume hood overnight and then placed under vacuum for 6–8 h to remove all residual solvent. Films were then hydrated by adding 6 μL of deuterium-depleted water to each plate and then placing the plates in a sealed chamber containing saturated ammonium phosphate solution (65 g/250 mL) at room temperature for 4 days. The mica plates were then stacked with an empty plate of the same dimensions placed over the top plate. The stacked plates were then wrapped with thin plastic film and

heat-sealed into a polyethylene envelope containing an additional 8–10 μL of deuterium-depleted water to maintain hydration. Samples were then allowed to equilibrate for 2 days to ensure homogeneous hydration prior to the initiation of NMR observations. At least two independent oriented samples were prepared and examined for each peptide-containing bilayer mixture to ensure that the observed spectra were characteristic of that composition. The absence of significant hydrolysis in similarly hydrated samples of POPC-d_{31}/POPG with and without SP-$B_{63–78}$ was previously demonstrated using thin-layer chromatography (Yang et al. 2009).

BLES was extracted from saline dispersion using the method of Bligh and Dyer (1959). Specifically, 9 mg of BLES was transferred from 400 μL into 2 mL of $CHCl_3$/MeOH (2:1) by mixing and phase separation. DPPC-d_{62} (2.5 % by weight) and, for specific samples, peptide (1 mol%) were then added to the BLES-containing organic phase. The resulting mixture was then dried under a stream of nitrogen gas for 40–60 min before being redissolved in 150 μL of $CHCl_3$/MeOH (1:1). Preparation of mechanically oriented samples by deposition of this solution onto mica plates then proceeded as described above.

Multilamellar vesicle samples were prepared by transferring $CHCl_3$/MeOH (2:1) solutions of lipid or lipid plus peptide, as described above, into a round-bottom flask from which solvent was then removed by rotary evaporation followed by several hours of pumping. The resulting film was hydrated by adding 300–400 μL of deuterium-depleted water, in ~50 μL steps, while gently rotating the flask.

^{2}HNMR spectra were acquired at 400 MHz using a locally assembled 9.4-T spectrometer running a quadrupole echo pulse sequence (Davis et al. 1976) with $\pi/2$ pulses of length 4–4.25 μs separated by a 30 μs pulse delay. Depending on the sample geometry, the probe was fitted with either a horizontally mounted flat coil or an 8-mm-diameter cylindrical coil. Free induction decays for samples based on either POPC-d_{31}/POPG or BLES/DPPC-d_{62} were obtained by averaging 10,000–50,000 or 200,000–300,000 transients, respectively. These were collected with a repetition time of 0.9 s and oversampling (Prosser et al. 1991) to give an effective dwell time of 4 μs. For samples containing POPC-d_{31}/POPG or BLES, sample temperatures were regulated at 23 or 35 °C, respectively, using a Lakeshore Cryogenics (Westerville, OH) model 325 temperature controller.

^{31}P NMR studies of oriented and unoriented samples were performed on a Bruker Avance II 14.1-T (600 MHz) spectrometer operating at 243.04 MHz. For all ^{31}P studies, samples were inserted in a dual-tuned cross-polarization flat-coil probe which, for oriented bilayers, was positioned such that the bilayer normal was parallel to the external magnetic field. Phosphorus spectra were acquired with a $\pi/2$ pulse length of 11.5 μs, a recycle delay of 5 s, and 43 kHz proton decoupling. Depending on the signal-to-noise ratio, 4,000–10,000 transients were averaged for each ^{31}P spectrum. Chemical shifts were referenced externally to 85 % H_3PO_4, which was set to 0 ppm.

To illustrate the effect of mosaic spread on the spectra of mechanically oriented POPC-d_{31}/POPG spectra, oriented spectra with different levels of mosaic spread were simulated using the Octave programming environment (Eaton 2002). Orientational order parameters were adjusted to match those determined from a vesicle sample of POPC-d_{31}/POPG at 23 °C. Line broadening was adjusted such that line widths in the simulation for perfect alignment approximated those for the oriented peptide-free POPC-d_{31}/POPG sample. Mosaic spread was modeled by calculating spectral contributions at 1° steps in the angle β between the bilayer normal and the applied magnetic field, and weighting each contribution to the resulting spectrum using a Gaussian distribution characterized by width σ_β.

Results

Figure 2 shows ^{2}H NMR spectra obtained, at 23 °C, from multilamellar vesicle dispersions of POPC-d_{31}/POPG (7:3) with no peptide added (Fig. 2a), with 1 mol% Mini-B (Fig. 2b), and with the same molar amount of peptide but as separate SP-$B_{8–25}$ and SP-$B_{63–78}$ fragments (Fig. 2c). Proton-decoupled ^{31}P spectra of the same samples are shown in Fig. 2d–f, respectively.

The ^{2}H NMR spectra in Fig. 2a–c are characteristic of fully deuterated, saturated acyl chains on phospholipids undergoing fast, axially symmetric reorientation about a spherical distribution of bilayer normal directions in a multilamellar vesicle dispersion of liquid-crystalline lipid bilayers. Each spectrum is a superposition of Pake doublets, each corresponding to a deuterated chain segment. The quadrupole splitting, measured between the prominent edges of each doublet, is given by

$$\Delta\nu = \frac{3}{4}\frac{e^2qQ}{h}S_{CD}, \quad (1)$$

where S_{CD} is the orientational order parameter for that segment and $(e^2qQ)/h$ = 167 kHz is the quadrupole coupling constant for a carbon–deuteriumbond. The orientational order parameter for a given segment is

$$S_{CD} = \frac{1}{2}\left\langle 3\cos^2\theta_{CD} - 1\right\rangle, \quad (2)$$

where θ_{CD} is the angle between the carbon–deuterium bond and the bilayer normal, and the average denoted by the angle brackets is over accessible chain conformations. The largest quadrupole splittings in the ^{2}H NMR spectra correspond to relatively ordered chain segments near the headgroup end of the acyl chain where motions are most restricted. Quadrupole splittings and segment orientational order decrease along the chain, reflecting the less constrained chain motion near the bilayer center. The prominent doublet at the smallest splitting arises from the chain methyl group. The dependence of chain orientational order on position along the chain is characterized by an orientational order parameter profile (Seelig and Seelig 1977, 1980; Davis 1983). An approximation of the orientational order parameter profile, referred to as a smoothed order parameter profile, can be extracted from the spectrum of a fully deuterated chain in a vesicle sample by assuming monotonic dependence of the orientational order parameter on segment position along the chain (Lafleur et al. 1989). Figure 2g shows smoothed order parameter profiles corresponding to the spectra in Fig. 2a–c.

Comparison of the ^{2}H spectra and order parameter profiles in Fig. 2 shows little perturbation of POPC-d_{31} chain orientational order by either Mini-B or its component helices separately. This is reminiscent of previous studies in which full-length SP-B and SP-$B_{8–25}$ were found to have limited effects on acyl chain orientational order in multilamellar vesicle model surfactant systems (Morrow et al. 2007; Russell-Schulz et al. 2009).

The ^{31}P spectra for POPC-d_{31}/POPG with and without the peptides present (Fig. 2d–f) are superpositions of anisotropic chemical shift powder patterns for the two lipid species present. Each of the component powder patterns is characteristic of fast axially symmetric headgroup reorientation about the bilayer normal. In each case, the more intense component is presumed to arise from POPC-d_{31} in the mixture. Comparison of the ^{31}P spectra in Fig. 2 suggests that Mini-B has almost no effect on average headgroup orientation while the mixture of its component helices has a small effect.

Application of a dePakeing algorithm to the ^{2}H NMR spectrum of a multilamellar vesicle dispersion yields the spectrum that would be obtained for a sample having the same distribution of orientational order parameters but with bilayer normal aligned along the magnetic field. Because bilayer normals in a vesicle sample are randomly oriented, vesicle spectra, and thus the corresponding dePaked spectra, are insensitive to additional convolutions of the bilayer surface, on a length scale large enough to preclude motional averaging by diffusion, as long as the overall randomness of the bilayer normal distribution is conserved. On the other hand, spectra from samples that are mechanically oriented by, for example, mica plates, are quite sensitive to departures from average bilayer orientation on such length scales. Figure 3 compares dePaked transforms of the ^{2}H NMR spectra in Fig. 2 with spectra from the mechanically oriented bilayer samples that were prepared with the same POPC-d_{31}/POPG/peptide compositions.

In the absence of peptide, both the dePaked vesicle and oriented sample spectra (Fig. 3a and b, respectively) are superpositions of doublets at the quadrupole splittings, for each chain segment, corresponding to axially symmetric chain reorientation about a bilayer normal oriented parallel to the applied magnetic field. The intense doublet at the largest splitting corresponds to the headgroup end of the chain where orientational order changes only slightly with position along the chain giving rise to a characteristic plateau in the orientational order parameter. The vertical line at 25 kHz in Fig. 3 facilitates comparison of the plateau splittings in the dePaked and oriented sample spectra.

Quadrupole splittings in the peptide-free oriented sample spectrum (Fig. 3b) are about 9 % larger than in the corresponding dePaked vesicle spectrum (Fig. 3a). Using a series of mechanically oriented samples prepared with different amounts of lipid per mica plate, it was found that the oriented sample splittings approached those of the corresponding dePaked vesicle spectrum as the amount of lipid per plate increased (results not shown). It is thus likely that the difference between Fig. 3a and b reflects a small additional ordering due to the proximity of the mica plate. The lines forming each doublet in the oriented sample spectrum (Fig. 3b) are only slightly wider than those in the corresponding dePaked vesicle sample spectrum (Fig. 3a), indicating that departures from perfect alignment in the mechanically oriented peptide-free sample must be small.

The spectra for the sample containing the mixture of SP-$B_{8–25}$ and SP-$B_{63–78}$ (Figs. 3e and 2f) also display slight differences in quadrupole splittings and little difference in the widths of component lines. In the oriented sample spectrum (Fig. 3f), however, an underlying base of additional intensity between ± 12.5 kHz indicates the presence of a broad spectral component. As discussed below, this is presumably a small misoriented fraction of the sample that is not in rapid exchange with the predominant oriented fraction.

The ^{2}H NMR spectrum obtained from the mechanically oriented POPC-d_{31}/POPG sample containing 1 mol% Mini-B (Fig. 3d) was significantly different from the corresponding dePaked vesicle sample spectrum (Fig. 3c) and from the spectra of the other mechanically oriented POPCd_{31}/POPG samples (Fig. 3b, f). As noted above, the characteristics of the oriented-sample POPC-d_{31}/POPG/peptide spectra were confirmed using independently prepared samples.

The presence of intensity at splittings between ±12.5 and ±25 kHz in Fig. 3d demonstrates that this sample is oriented with bilayer normals, on average, parallel to the magnetic field. The doublets at splittings greater than ±12.5 kHz, however, are broadened in a way that is characteristic of a wide distribution, or mosaic spread, of bilayer normal directions about the magnetic field direction. The presence of significant additional intensity between ±12.5 kHz and the appearance of a small doublet at half of the oriented-sample methyl doublet splitting

indicates a population of bilayers with normal oriented perpendicular to the magnetic field. An independent population of randomly oriented bilayers could give rise to a spectral component with intensity between ±12.5 kHz, but a distribution of bilayer normal directions wide enough to account for the line broadening seen in the oriented bilayer doublets with splittings between ±12.5 and ±25 kHz is also expected to give rise to enhanced intensity of the spectrum at splittings less than ±12.5 kHz. This is illustrated by simulations shown in Fig. 4.

The simulations of oriented POPC-d_{31} spectra in Fig. 4 illustrate the effect of increasing levels of mosaic spread on the distribution of intensity across the ^{2}H NMR spectrum. In the absence of information about the shape of bilayer protrusions or misalignment, the distribution of bilayer normal orientations about the magnetic field direction has been modeled by a Gaussian distribution of the angle, β, between the bilayer normal and the magnetic field direction, with characteristic widths as indicated on the figure. This is likely an oversimplification, and the values of σ_β indicated should not be taken as quantitative characterizations of the mosaic spread corresponding to a particular spectral shape. Nevertheless, the simulations do illustrate how small levels of mosaic spread broaden individual doublets and how larger levels of mosaic spread can give rise to enhanced intensity bounded by the splitting corresponding to plateau deuterons in bilayers with normals oriented perpendicular to the magnetic field. The emergence of spectral edges, at about ±12.5 kHz, with increasing mosaic spread, reflects the fact that splittings are proportional to $(3\cos^2\beta - 1)/2$, which is limited to values between −0.5 and 1. Any distribution of bilayer normal orientations wide enough to include a nonzero population of bilayer normals oriented perpendicular to the magnetic field must give rise to intensity edges at half the oriented spectrum maximum splitting.

Regardless of whether the enhanced central intensity in Fig. 3d reflects a superposition of well-oriented and randomly oriented bilayers, a broad distribution of bilayer normals about an average orientation along the magnetic field, or a combination of both, the spectral shape reflects heterogeneous broadening of the component spectral doublets. The spectra are, however, not indicative of a reduction in doublet splitting that would indicate averaging of the quadrupole interaction by diffusional sampling of different bilayer orientations by lipids over timescales shorter than the characteristic timescale for the ^{2}H NMR experiment (approximately 10^{-5} s). This indicates that Mini-B interferes with the orientation of POPC-d_{31}/POPG bilayers on length scales that are long enough to preclude lipid exchange on the ~10^{-5} s timescale of the ^{2}H NMR experiment. For most of the sample, splittings are reduced only slightly from those for the oriented bilayer and bilayer normal orientations remain close to the sample average. For a fraction of the POPCd_{31}/POPG sample, however, the interaction with SP-B results in much larger departures from average bilayer orientation.

Figure 5 shows ^{31}P NMR spectra of the oriented POPCd_{31}/POPG (7:3) bilayers without peptide and with the mixture of separated Mini-B component helices. Corresponding ^{31}P NMR spectra of the oriented POPC-d_{31}/POPG (7:3) bilayers with Mini-B were not obtained due to technical difficulties with the flat-coil ^{31}P probe over the period during which fresh samples were available. The ^{31}P spectrum of the mechanically oriented POPC-d_{31}/POPG sample (Fig. 5a) is characteristic of bilayers with normal directions fully oriented parallel to the magnetic field. The small feature at negative chemical shift in the spectrum of Fig. 5b may arise from the small fraction of the sample that also gives rise to the small underlying intensity between ±12.5 kHz in the ^{2}H spectrum of Fig. 3f. There is a small difference between the width of the main peak at 35.8 ppm in Fig. 5b and that of the peak at 37.1 ppm in Fig. 5a. This difference might correspond to the small change in mosaic spread indicated by comparison of the corresponding ^{2}H NMR spectra (Fig. 3f, b), or it might reflect a slight broadening of the distribution of phospholipid headgroup orientations in the presence of SP-

$B_{8–25}$ and SP-$B_{63–78}$. Aside from that difference, however, the similarity of the spectra of Fig. 5a and b indicates that the mixture of SP-$B_{8–25}$ and SP-$B_{63–78}$ has little effect on average phospholipid headgroup conformation.

Similar experiments were carried out using the natural surfactant, BLES, which retains all of the polar and charged lipid content of natural surfactant (Yu et al. 1983; Yu and Possmayer 1996) and in which 1–2 % of the dry weight is accounted for by the hydrophobic surfactant proteins SP-B and SP-C (Panda et al. 2007; Zuo et al. 2008). Earlier ^{2}H NMR observations of BLES doped with DPPC-d_{62} showed spectra characteristic of axially symmetric reorientation, corresponding to liquid-crystalline behavior, above ~31 °C and broader spectra, characteristic of gel, below 20 °C (Nag et al. 2006). Spectra at intermediate temperatures suggested a continuous phase change which was consistent with corresponding differential scanning calorimetry (DSC) scans.

The left panel of Fig. 6 shows ^{2}H NMR spectra, collected at 35 °C, for BLES doped with 2.5 % (w/w) DPPC-d_{62} with no peptide added (Fig. 6a), with 1 mol%SP-B (Fig. 6b), and with the same amount of peptide but as separate SP-$B_{8–25}$ and SP-$B_{63–78}$ fragments (Fig. 6c). Proton-decoupled ^{31}P spectra of the same samples are shown in Fig. 6d–f, respectively. Individual doublets in the ^{2}H NMR spectra of Fig. 6 are not as well resolved as in the model lipid mixture, but all three are characteristic of fast, axially symmetric lipid reorientation about a spherical distribution of bilayer normal directions, as expected for a multilamellar vesicle dispersion of liquid-crystalline bilayers. The poor doublet resolution in spectra of liquid-crystalline BLES/DPPC-d_{62}, which was also seen in the earlier study of this mixture (Nag et al. 2006), likely indicates that the characteristic time for exchange of DPPC-d_{62} between different environments in the complex BLES mixture is close to the upper limit for fast, axially symmetric reorientation.

The small narrow lines at the center of the BLES/DPPCd_{62} ^{2}H spectra in Fig. 6a–c likely reflect the presence of some DPPC-d_{62} in small, isotropically reorienting particles. Similar features were also seen in an earlier study of BLES/DPPC-d_{62}. The phospholipid component of BLES is dominated by phosphatidylcholines and phosphatidylglycerols and the ^{31}P spectra in the right panel of Fig. 6 reflect a mixture of phospholipid species in multilamellar vesicle dispersions. The ^{31}P spectra of the BLES samples containing peptides also have small features with chemical shift close to 0. As was the case for the model lipid mixture, comparison of the spectra in Fig. 6 suggests that the addition of Mini-B, or a mixture of its helix components, at the low concentrations used here has little effect on average DPPC-d_{62} acyl chain orientational order in the BLES mixtures.

The observation of small peaks close to 0 ppm in ^{31}P NMR spectra may reflect a fraction of the sample in the form of small, isotropically reorienting particles or a fraction of the sample undergoing fast diffusion around highly curved structures. After a period of storage, thinlayer chromatography was used to compare the BLES/DPPC-d_{62}/Mini-B and BLES/DPPC-d_{62} samples from which the ^{31}P NMR spectra of Fig. 6e and d, respectively, were obtained. While comparison of these chromatograms (not shown) did not conclusively rule out lipid hydrolysis, their similarity suggests that hydrolysis alone is unlikely to account for the presence of a peak near 0 ppm in the ^{31}P spectrum of BLES/DPPC-d_{62}/Mini-B (Fig. 6e) and the absence of such a peak in the corresponding spectrum of BLES/DPPC-d_{62} (Fig. 6d). It is interesting to note that the peak at 0.7 ppm in the ^{31}P spectrum of Fig. 6e accounts for a larger fraction of the spectral area than the narrow central peak in the corresponding ^{2}H spectrum of Fig. 6b. This may indicate that the concentration of DPPC-d_{62} in the part of the sample giving rise to the peak at 0.7 ppm in the ^{31}P spectrum of Fig. 6e is lower than in the bulk of the BLES/DPPC-d_{62} sample, but the current experiments leave this question unresolved.

The left panel of Fig. 7 shows ^{2}H NMR spectra obtained from mechanically oriented bilayers of BLES/DPPC-d_{62} with no peptide, with 1 mol% Mini-B, and with the same amount of peptide as a mixture of the SP-$B_{8–25}$ and SP-$B_{63–78}$ components of Mini-B. Again, the characteristics of the oriented-sample BLES/DPPC-d_{62} spectra were confirmed using independently prepared samples. The right panel of Fig. 7 shows corresponding ^{31}P spectra for the oriented BLES/DPPC-d_{62} samples.

The breadth of individual doublets in Fig. 7a suggests that, even without peptide, BLES/DPPC-d_{62} bilayers were not as well oriented as the peptide-free POPC-d_{31}/POPG bilayers. Comparison of Fig. 7a and b, however, shows that addition of Mini-B did not significantly perturb the distribution of BLES bilayer orientations. This differs from the response of the oriented POPC-d_{31}/POPC mixture to the addition of Mini-B but may reflect the more complex lipid composition of BLES or the presence of some SP-B and SP-C in the original BLES mixture.

Figure 7c, on the other hand, shows that addition of Mini-B component helices as a mixture of SP-$B_{8–25}$ and SP-$B_{63–78}$ did broaden the distribution of BLES/DPPC-d_{62} bilayer orientations. As was seen when Mini-B was added to POPC-d_{31}/POPG, the addition of the SP-$B_{8–25}$/SP-$B_{63–78}$ mixture to BLES/DPPC-d_{62} induced a broadening of doublet lines at splittings close to the maximum oriented bilayer splitting and the appearance of spectral intensity for splittings less than half the maximum oriented bilayer splitting. As before, this indicates an increase in width of the bilayer normal orientational distribution and possibly some randomly oriented bilayer material. Again, as noted above, the characteristics of oriented-sample BLES/DPPC-d_{31}/peptide spectra were confirmed using independently prepared samples.

The ^{31}P NMR spectra of oriented BLES/DPPC-d_{62} with no peptide (Fig. 7d) and with 1 mol % Mini-B (Fig. 7e) are consistent with predominant alignment of bilayer normal along the magnetic field direction. In the ^{31}P NMR spectra of oriented BLES/DPPC-d_{62} with the SP-$B_{8–25}$/SP-$B_{63–78}$ mixture (Fig. 7f), the appearance of a distinct feature at negative chemical shift is consistent with the indications of an unoriented fraction in the corresponding ^{2}H NMR spectrum.

Discussion

The observations reported here illustrate aspects of interactions between SP-B constructs and lipids that are of potential relevance to the understanding of lung surfactant function. Before relating this work to previous studies, some comment on how peptide levels employed in various model studies compare with those in natural surfactant may be helpful. In bovine surfactant, SP-B accounts for about 0.5 % of the surfactant dry weight and there are about 4,200 phospholipids per SP-B dimer (Zuo et al. 2008). At protein-to-lipid ratios of about 0.2 mol%, Mini-B and its separate component helices display significant activity in both captive bubble surfactometry and in lung oxygenation measurements performed on surfactant-deficient rats (Waring et al. 2005). In studies using much higher levels of SP-B and peptides derived from SP-B, observations of significantly perturbed phospholipid acyl chain average orientational order have provided some insights into the interaction of SP-B with the lipid components of surfactant (Morrow et al. 2004; Antharam et al. 2008; Farver et al. 2010). There is, however, evidence from captive bubble surfactometry that film stability is reduced by total protein (SP-B and SP-C) concentrations in excess of about 2 % by weight (Schürch et al. 2010).

The peptide fractions of 1 mol% used in this work correspond to about 5 % by dry sample weight and are thus slightly higher than physiological levels but lower than peptide amounts

at which there is significant perturbation of average phospholipid acyl chain orientational order. Despite the critical dependence of lung surfactant function on the presence of SP-B, observed effects of SP-B on lipid properties at small length scales, as represented by its effects on average chain orientational order in previous studies, have been small when protein-to-lipid ratios are low (Dico et al. 1997). When present separately, the SP-B fragments SP-$B_{8–25}$ and, at low (nearly physiological) concentration, SP-$B_{63–78}$ have also induced only small effects on lipid chain orientational order in surfactant model bilayers (Russell-Schulz et al. 2009; Yang et al. 2009). The present work also finds little perturbation of lipid chain average orientational order by the SP-B construct, Mini-B, or by a mixture of its component helices, SP-$B_{8–25}$ and SP-$B_{63–78}$. This indicates that these peptides have only small effects on the conformation of individual lipids or on the amplitude of local lipid motions. In light of the effectiveness with which Mini-B can support blood oxygenation levels in surfactant-deficient rats (Waring et al. 2005), these observations suggest that the functional role of Mini-B or, by extension, SP-B in surfactant might reflect more than just a substantial peptide-induced perturbation of orientational order.

In contrast, SP-B and its components have been found to significantly affect motions that influence quadrupole echo decay times in the liquid-crystalline phase (Dico et al. 1997), suggesting perturbations of longer-range motions such as collective motions. In the current work, incorporation of Mini-B into surfactant model lipid bilayers constrained by mica plates broadened the distribution of bilayer normal directions about the average normal orientation and also gave rise to a nonoriented bilayer fraction. A mixture of the Mini-B component helices was found to similarly affect mica-constrained bilayers of the nearly complete natural surfactant, BLES. The observation of heterogeneously broadened lines and of significant departures from average bilayer orientation, rather than changes in doublet splittings, indicates that departures from average orientation took place over length scales that were long enough to preclude averaging by lateral lipid diffusion. The area sampled by a diffusing lipid during the characteristic time, τ, of a ^{2}H NMR experiment is $A = 4\pi D_L \tau$, where D_L is the lipid lateral diffusion constant (Davis 1983). Using an estimate of $D_L \approx 10 \times 10^{-12}$ m^2/s from pulsed field gradient NMR results (Filippov et al. 2003; Almeida et al. 2005) and a characteristic time $\tau \approx 10^{-5}$ s, the areas over which bilayer orientations depart from average in the perturbed spectra are thus estimated to be greater than ~1,200 nm^2.

The propensity for Mini-B or the mixture of SP-$B_{8–25}$ and SP-$B_{63–78}$ to promote significant departures from average orientation in mica-constrained bilayers presumably reflects a peptide-induced modification of the energetic cost associated with bilayer misalignment in a mechanically oriented sample. These samples are prepared by deposition of the lipid or lipid–peptide solution on mica plates followed by drying, hydration, and stacking of the plates. Samples which display perturbed alignment presumably contain unaligned bilayers at the hydration stage prior to stacking but must also resist alignment resulting from confinement by the mica plates. The peptide-free samples which display more complete alignment are either better aligned in the hydration stage or can more freely respond to the orienting influence of the mica plates upon stacking. Regardless of whether the effect of the peptide is primarily felt at the stacking stage or at both the hydration and stacking stages of the alignment process, the resulting misalignment might be considered to amount to the introduction of defects into planar bilayer stacks. One way to imagine this happening would be if peptide-induced coupling of adjacent bilayers at the hydration stage were to promote the persistence of protrusions and/or large-scale bilayer corrugations which could then be trapped when the bilayers were more confined in the stack of mica plates. Possible mechanisms for such coupling might include direct linking of adjacent bilayers by shared peptides or the bridging of adjacent bilayers by peptide-stabilized stalk structures.

These observations suggest that Mini-B and its component peptides interact with some bilayers in a way that can inhibit bilayer response to the orienting constraint imposed by flat supporting surfaces. However, it is not straightforward to correlate surfactant function with the misalignment of mechanically constrained bilayers on the large length scales implied by the observation of significant additional intensity between ±12.5 kHz. The fact that the two lipid mixtures studied here responded differently to the two peptide mixtures suggests that the extent to which Mini-B or its component peptides can promote or stabilize departures from bilayer flatness during the mechanical orientation process is sensitive to details of the bilayer composition, including the degree of lipid chain saturation and the presence of native hydrophobic protein, and the peptide structure. In particular, BLES/DPPC-d_{62}, which naturally contains SP-B, does not orient as fully as peptidefree POPC-d_{31}/POPG but also does not display significant additional intensity between ±12.5 kHz even with the addition of 1 mol% Mini-B. It should also be noted that the difference between the gel-to-liquid crystalline transition temperature and the temperatures at which observations were made was much larger for the POPC-d_{31}/POPG samples than for the BLES/DPPC-d_{62} samples.

The observation of enhanced intensity between ±12.5 kHz reflects the presence of bilayers with normals oriented perpendicular to the magnetic field over length scales large enough to preclude averaging by exchange of diffusing lipids with better oriented fractions. This implies the presence and stability of defects that presumably perturb stacking over multiple bilayers. Such defects or protrusions may be stabilized by interactions that also contribute to bilayer coupling in functional surfactant mixtures, but it may be the scale of the resulting misalignment that is sensitive to bilayer composition; For example, bilayer coupling defects, resulting from local stalk formation or direct peptide-mediated bridging, might be accommodated with little effect on macroscopic bilayer alignment if distributed uniformly through an oriented three-dimensional bilayer stack. Clustering of such defects, on the other hand, might disrupt local packing sufficiently to give rise to the observations of significant mosaic spread. Such effects might account for the differences between the observed responses of POPC-d_{31}/POPG and BLES/DPPC-d_{62} to 1 mol% (5 wt.%) Mini-B or the responses of BLES/DPPC-d_{62} to Mini-B or the same amount of peptide present as separate helices. In this regard, it is interesting that, in a previous study of SP-$B_{63–78}$ alone in bilayers, SP-$B_{63–78}$ alone consistently induced spectral features consistent with perpendicular bilayer normal orientations at concentrations above 2.5 wt.% (Yang et al. 2009).

Notwithstanding their apparent sensitivity to bilayer composition, the observations reported here do provide some insight into how it might be possible to reconcile SP-B's limited effect on local lipid conformation with its essential contribution to lung surfactant function, and thus, presumably, to the important lipid reorganizations implicit in that function. As noted above, the observation of fractions with large departures from average orientation in some samples indicates lipid population heterogeneity on length scales that preclude averaging by diffusion on the spectral timescale. This suggests that interactions, between SP-B components and lipids in some mixtures, can compete with the interactions responsible for flattening bilayers in mechanically oriented samples, thereby promoting departures from planar geometry over large length scales. Proper functioning, and maintenance, of lung surfactant requires the recruitment of surfactant material into the surface-active layer from adjacent bilayer reservoirs, and the transfer of material to such reservoirs as lung volume varies (Zuo et al. 2008; Rugonyi et al. 2008; Possmayer et al. 2010; Frey et al. 2010). This implies a need for close contacts between bilayers and surface layers. The observation of increased mosaic spread and large departures from average orientation in some mechanically oriented peptide-containing samples might reflect the stabilization of protrusions or bilayer packing defects resulting from the linking of adjacent bilayers by peptide-induced stalks. While differences in scale cannot be dismissed, it may be that similar departures from

bilayer flatness facilitate the close contact between bilayers and surface layers required in functional surfactant. Important details of the interactions between SP-B-derived peptides and bilayers or surfactant remain unresolved, but these observations do suggest that such interactions may promote collective perturbations of large bilayer surface areas.

Acknowledgments

This work was supported by the Canadian Institutes of Health Research and by the Natural Sciences and Engineering Research Council of Canada, and by the National Institutes of Health (HL-094641). We acknowledge the CREAIT network at Memorial for assisting with NMR facility maintenance and training, and in particular Dr. Celine Schneider. We would like to thank Lauren MacEachern for her help with the simulations, Donna Jackman for her help with sample preparation, as well as Frans Walther for the assistance he provided.

References

Almeida PF, Vaz WL, Thompson TE. Lipid diffusion, free area, and molecular dynamics simulations. Biophys J. 2005; 88:4434–4438. [PubMed: 15805166]

Antharam VC, Farver RS, Kuznetsova A, Sippel KH, Mills FD, Elliott DW, Sternin E, Long JR. Interactions of the C-terminus of lung surfactant protein B with lipid bilayers are modulated by acyl chain saturation. Biochim Biophys Acta. 2008; 1778:2544–2554. [PubMed: 18694722]

Baatz JE, Sarin V, Absolom DR, Baxter C, Whitsett JA. Effects of surfactant-associated protein SP-B synthetic analogs on the structure and surface activity of model membrane bilayers. Chem Phys Lipids. 1991; 60:163–178. [PubMed: 1814640]

Bertani P, Vidovic V, Yang TC, Rendell J, Gordon LM, Waring AJ, Bechinger B, Booth V. Orientation and depth of surfactant protein B C-terminal helix in lung surfactant bilayers. Biochim Biophys Acta. 2012; 1818:1165–1172. [PubMed: 22252270]

Bligh EG, Dyer WJ. A rapid method of total lipid extraction and purification. Can J Biochem Physiol. 1959; 37:911–917. [PubMed: 13671378]

Booth VK, Waring AJ, Walther FJ, Keough KM. NMR structures of the C-terminal segment of surfactant protein B in detergent micelles and hexafluoro-2-propanol. Biochemistry. 2004; 43:15187–15194. [PubMed: 15568810]

Clark JC, Wert SE, Bachurski CJ, Stahlman MT, Stripp BR, Weaver TE, Whitsett JA. Targeted disruption of the surfactant protein B gene disrupts surfactant homeostasis, causing respiratory failure in newborn mice. Proc Natl Acad Sci USA. 1995; 92:7794–7798. [PubMed: 7644495]

Crouch EC. Structure, biologic properties, and expression of surfactant proteinD(SP-D). Biochim Biophys Acta. 1998; 1408:278–289. [PubMed: 9813367]

Davis JH. The description of membrane lipid conformation, order and dynamics by 2H-NMR. Biochim Biophys Acta. 1983; 737:117–171. [PubMed: 6337629]

Davis JH, Jeffrey KR, Bloom M, Valic M, Higgs TP. Quadrupolar echo deuteron magnetic resonance spectroscopy in ordered hydrocarbon chains. Chem Phys Lett. 1976; 42:390–394.

Dico AS, Hancock J, Morrow MR, Stewart J, Harris S, Keough KM. Pulmonary surfactant protein SP-B interacts similarly with dipalmitoylphosphatidylglycerol and dipalmitoylphosphatidylcholine in phosphatidylcholine/phosphatidylglycerol mixtures. Biochemistry. 1997; 36:4172–4177. [PubMed: 9100011]

Eaton, JW. Gnu Octave manual. Network Theory Limited; Bristol: 2002.

Farver RS, Mills FD, Antharam VC, Chebukati JN, Fanucci GE, Long JR. Lipid polymorphism induced by surfactant peptide SP-B_{1-25}. Biophys J. 2010; 99:1773–1782. [PubMed: 20858421]

Filippov A, Oradd G, Lindblom G. The effect of cholesterol on the lateral diffusion of phospholipids in oriented bilayers. Biophys J. 2003; 84:3079–3086. [PubMed: 12719238]

Frey SL, Pocivavsek L, Waring AJ, Walther FJ, Hernandez-Juviel JM, Ruchala P, Lee KYC. Functional importance of the NH2-terminal insertion sequence of lung surfactant protein B. Am J Physiol Lung Cell Mol Physiol. 2010; 298:L335–L347. [PubMed: 20023175]

Goerke J. Pulmonary surfactant: functions and molecular composition. Biochim Biophys Acta. 1998; 1408:79–89. [PubMed: 9813251]

Hawgood S, Derrick M, Poulain F. Structure and properties of surfactant protein B. Biochim Biophys Acta. 1998; 1408:150–160. [PubMed: 9813296]

Hildebran JN, Goerke J, Clements J. Pulmonary surface film stability and composition. J Appl Physiol. 1979; 47:604–611. [PubMed: 583282]

Kang JH, Lee MK, Kim KL, Hahm KS. The relationships between biophysical activity and the secondary structure of synthetic peptides from the pulmonary surfactant protein SP-B. Biochem Mol Biol Int. 1996; 40:617–627. [PubMed: 8908373]

Kurutz JW, Lee KY. NMR structure of lung surfactant peptide SP-B(11-25). Biochemistry. 2002; 41:9627–9636. [PubMed: 12135384]

Lafleur M, Fine B, Sternin E, Cullis PR, Bloom M. Smoothed orientational order profile of lipid bilayers by 2H-nuclear magnetic resonance. Biophys J. 1989; 56:1037–1041. [PubMed: 2605294]

Lang CJ, Postle AD, Orgeig S, Possmayer F, Bernhard W, Panda AK, Jurgens KD, Milson WK, Nag K, Daniels CB. Dipalmitoylphosphatidylcholine is not the major surfactant phospholipid species in all mammals. Am J Physiol Regul Integr Comp Physiol. 2005; 289:R1426–R1439. [PubMed: 16037124]

Lindhout DA, Thiessen A, Schieve D, Sykes BD. High-yield expression of isotopically labeled peptides for use in NMR studies. Protein Sci. 2003; 12:1786–1791. [PubMed: 12876327]

Liu S, Zhao L, Manzanares D, Doherty-Kirby A, Zhang CJ, Possmayer F, Lajoie GA. Characterization of bovine surfactant proteins B and C by electrospray ionization mass spectrometry. Rapid Commun Mass Spectrom. 2008; 22:197–203. [PubMed: 18088070]

McCormack FX. Structure, processing and properties of surfactant protein A. Biochim Biophys Acta. 1998; 1408:109–131. [PubMed: 9813267]

Morrow MR, Stewart J, Taneva S, Dico A, Keough KMW. Perturbation of DPPC bilayers by high concentrations of pulmonary surfactant SP-B. Eur Biophys J. 2004; 33:285–290. [PubMed: 14504839]

Morrow MR, Temple S, Stewart J, Keough KM. Comparison of DPPC and DPPG environments in pulmonary surfactant models. Biophys J. 2007; 93:164–175. [PubMed: 17434940]

Nag K, Keough KMW, Morrow MR. Probing perturbation of bovine lung surfactant extracts by albumin using DSC and ^{2}H-NMR. Biophys J. 2006; 90:3632–3642. [PubMed: 16500977]

Nogee LM, Garnier G, Dietz HC, Singer L, Murphy AM, deMello DE, Colten HR. A mutation in the surfactant protein B gene responsible for fatal neonatal respiratory disease in multiple kindreds. J Clin Invest. 1994; 93:1860–1863. [PubMed: 8163685]

Panda AK, Nag K, Harbottle RR, Possmayer F, Petersen NO. Thermodynamic studies of bovine lung surfactant extract mixing with cholesterol and its palmitate derivative. J Colloid Interface Sci. 2007; 311:551–555. [PubMed: 17434181]

Pérez-Gil J. Molecular interactions in pulmonary surfactant films. Biol Neonate. 2002; 81(suppl 1):6–15. [PubMed: 12011560]

Perez-Gil J, Weaver TE. Pulmonary surfactant pathophysiology: current models and open questions. Physiology (Bethesda). 2010; 25:132–141. [PubMed: 20551227]

Possmayer F, Hall SB, Haller T, Petersen NO, Zuo YY, de la Serna JB, Postle AD, Veldhuizen RAW, Orgeig S. Recent advances in alveolar biology: some new looks at the alveolar interface. Respir Physiol Neurobiol. 2010; 173(Suppl):S55–S64. [PubMed: 20206718]

Postle AD, Heeley EL, Wilton DC. A comparison of the molecular species compositions of mammalian lung surfactant phospholipids. Comp Biochem Physiol Part A Mol Integr Physiol. 2001; 129:65–73.

Prosser RS, Davis JH, Dahlquist FW, Lindorfer MA. 2H nuclear magnetic resonance of the gramicidin A backbone in a phospholipid bilayer. Biochemistry. 1991; 30:4687–4696. [PubMed: 1709361]

Revak SD, Merritt TA, Hallman M, Heldt G, La Polla RJ, Hoey K, Houghten RA, Cochrane CG. The use of synthetic peptides in the formation of biophysically and biologically active pulmonary surfactants. Pediatr Res. 1991; 29:460–465. [PubMed: 1896249]

Rugonyi S, Biswas SC, Hall SB. The biophysical function of pulmonary surfactant. Respir Physiol Neurobiol. 2008; 163:244–255. [PubMed: 18632313]

Russell-Schulz B, Booth V, Morrow MR. Perturbation of DPPC/POPG bilayers by the N-terminal helix of lung surfactant protein SP-B: a (2)H NMR study. Eur Biophys J. 2009; 38:613–624. [PubMed: 19224204]

Ryan MA, Qi XY, Serrano AG, Ikegami M, Pérez-Gil J, Johansson J, Weaver TE. Mapping and analysis of the lytic and fusogenic domains of surfactant protein B. Biochemistry. 2005; 44:861–872. [PubMed: 15654742]

Sarker M, Waring AJ, Walther FJ, Keough KM, Booth V. Structure of Mini-B, a functional fragment of surfactant protein B, in detergent micelles. Biochemistry. 2007; 46:11047–11056. [PubMed: 17845058]

Schürch D, Ospina OL, Cruz A, Pérez-Gil J. Combined and independent action of proteins SP-B and SP-C in the surface behavior and mechanical stability of pulmonary surfactant films. Biophys J. 2010; 99:3290–3299. [PubMed: 21081077]

Seelig A, Seelig J. Effect of a single cis double bond on the structures of a phospholipid bilayer. Biochemistry. 1977; 16:45–50. [PubMed: 831777]

Seelig J, Seelig A. Lipid conformation in model membranes and biological membranes. Q Rev Biophys. 1980; 13:19–61. [PubMed: 7220788]

Serrano AG, Ryan M, Weaver TE, Pérez-Gil J. Critical structure-function determinants within the N-terminal region of pulmonary surfactant protein SP-B. Biophys J. 2006; 90:238–249. [PubMed: 16214863]

Walther FJ, Hernandez-Juviel JM, Gordon LM, Sherman MA, Waring AJ. Dimeric surfactant protein B peptide sp-b(1–25) in neonatal and acute respiratory distress syndrome. Exp Lung Res. 2002; 28:623–640. [PubMed: 12490037]

Walther FJ, Waring AJ, Hernandez-Juviel JM, Gordon LM, Schwan AL, Jung CL, Chang YS, Wang ZD, Notter RH. Dynamic surface activity of a fully synthetic phospholipase-resistant lipid/peptide lung surfactant. PLoS ONE. 2007; 2:e1039. [PubMed: 17940603]

Walther FJ, Waring AJ, Hernandez-Juviel JM, Gordon LM, Wang ZD, Jung CL, Ruchala P, Clark AP, Smith WM, Sharma S, Notter RH. Critical structural and functional roles for the N-terminal insertion sequence in surfactant protein B analogs. PLoS ONE. 2010; 5:e8672. [PubMed: 20084172]

Waring AJ, Walther FJ, Gordon LM, Hernandez-Juviel JM, Hong T, Sherman MA, Alonso C, Alig T, Braun A, Bacon D, Zasadzinski JA. The role of charged amphipathic helices in the structure and function of surfactant protein B. J Pept Res. 2005; 66:364–374. [PubMed: 16316452]

Whitsett JA, Nogee LM, Weaver TE, Horowitz AD. Human surfactant protein B: structure, function, regulation, and genetic disease. Physiol Rev. 1995; 75:749–757. [PubMed: 7480161]

Yang TC, McDonald M, Morrow MR, Booth V. The effect of a C-terminal peptide of surfactant protein B (SP-B) on oriented lipid bilayers, characterized by solid-state 2H- and 31P-NMR. Biophys J. 2009; 96:3762–3771. [PubMed: 19413982]

Yu SH, Possmayer F. Effect of pulmonary surfactant protein A and neutral lipid on accretion and organization of dipalmitoylphosphatidylcholine in surface films. J Lipid Res. 1996; 37:1278–1288. [PubMed: 8808762]

Yu S, Harding PG, Smith N, Possmayer F. Bovine pulmonary surfactant: chemical composition and physical properties. Lipids. 1983; 18:522–529. [PubMed: 6688646]

Zuo YY, Veldhuizen RA, Neumann AW, Petersen NO, Possmayer F. Current perspectives in pulmonary surfactant–inhibition, enhancement and evaluation. Biochim Biophys Acta. 2008; 1778:1947–1977. [PubMed: 18433715]

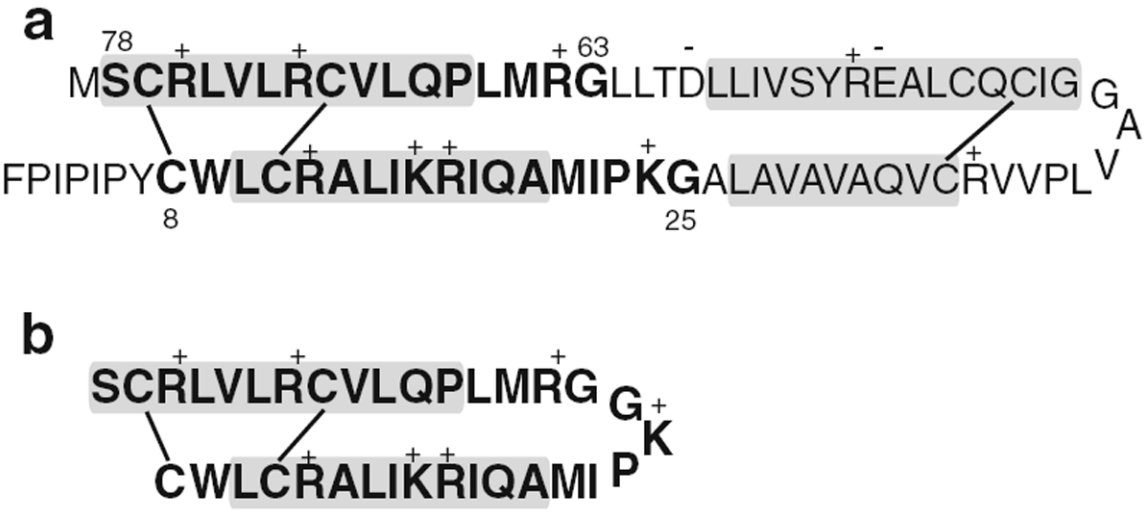

Fig. 1.

a The primary structure of human SP-B (Liu et al. 2008) showing the internal disulfide bonds. The residues included in the SP-B construct Mini-B are indicated in *bold*. The approximate locations of segments expected to be helical are indicated by *shaded boxes*. **b** The primary structure of Mini-B (Waring et al. 2005)

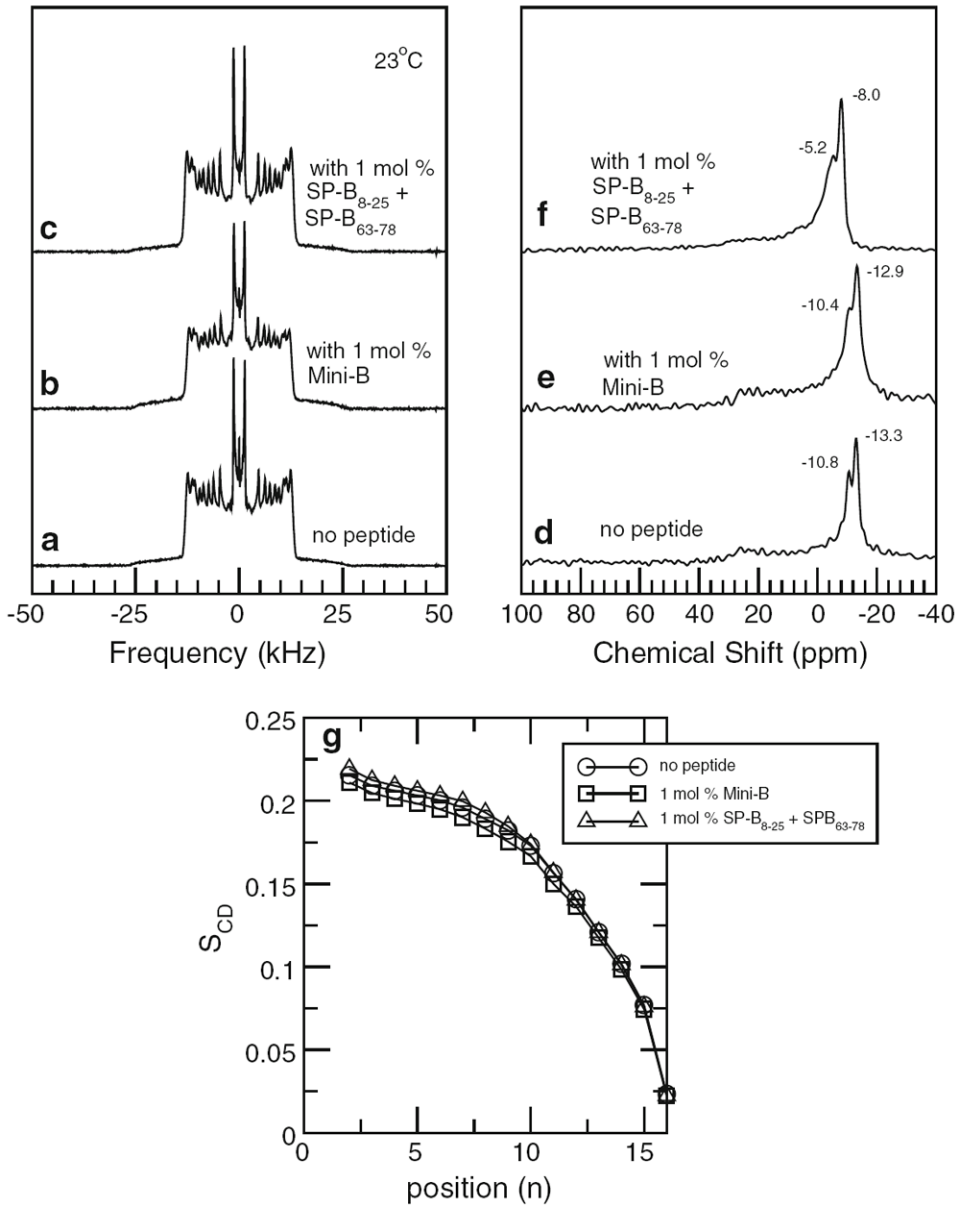

Fig. 2.

Top left panel ^{2}H NMR spectra of multilamellar vesicle dispersions containing POPC-d_{31}/POPG (7:3) with no peptide (*a*), 1 mol% Mini-B (*b*), and 1 mol% SP-$B_{8–25}$ and SP-$B_{63–78}$ peptide separately (*c*). *Top right panel* Corresponding ^{31}P NMR spectra of multilamellar vesicle dispersions containing POPC-d_{31}/POPG (7:3) with no peptide (*d*), 1 mol% Mini-B (*e*), and 1 mol% SP-$B_{8–25}$ and SP-$B_{63–78}$ peptide separately (*f*). *Bottom panel* (*g*) Smoothed orientational order parameter profiles derived from the ^{2}H NMR spectra of multilamellar vesicle dispersions containing POPC-d_{31}/POPG (7:3) with no peptide (circles), 1 mol% mini-B (*squares*), and 1 mol% SP-$B_{8–25}$ and SP-$B_{63–78}$ peptide separately (*triangles*). All data taken at 23 °C

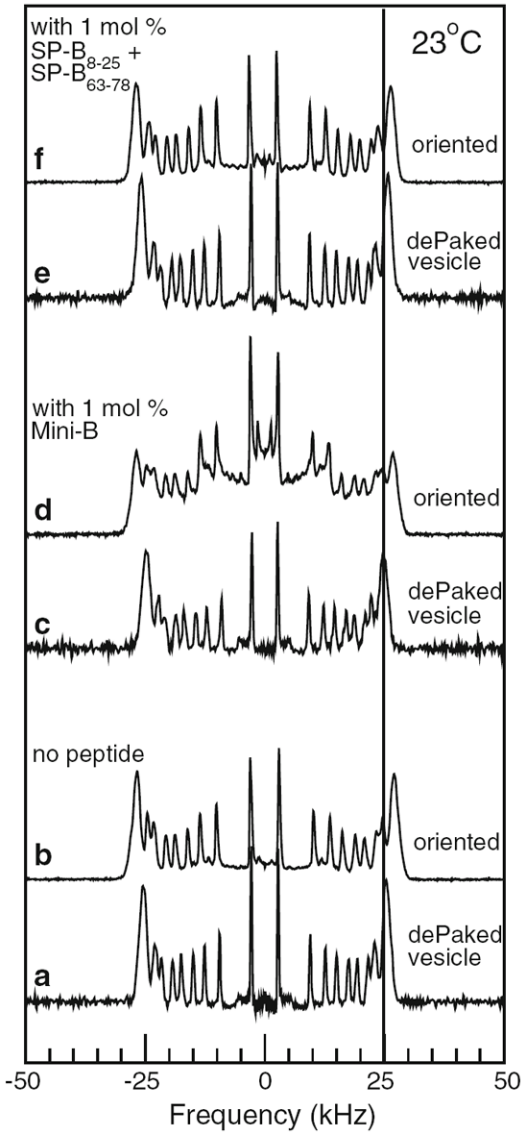

Fig. 3.

Comparison of ^{2}H NMR spectra from samples mechanically oriented with bilayer normals parallel to applied magnetic field (*b, d*, and *f*) and single-orientation spectra obtained by applying the dePakeing transform to multilamellar vesicle spectra (*a, c*, and *e*) for samples of POPC-d_{31}/POPG (7:3) with no peptide (*a, b*), 1 mol% Mini-B (*c, d*), and 1 mol% SP-$B_{8–25}$ and SP-$B_{63–78}$ peptide separately (*e, f*). All data taken at 23 °C

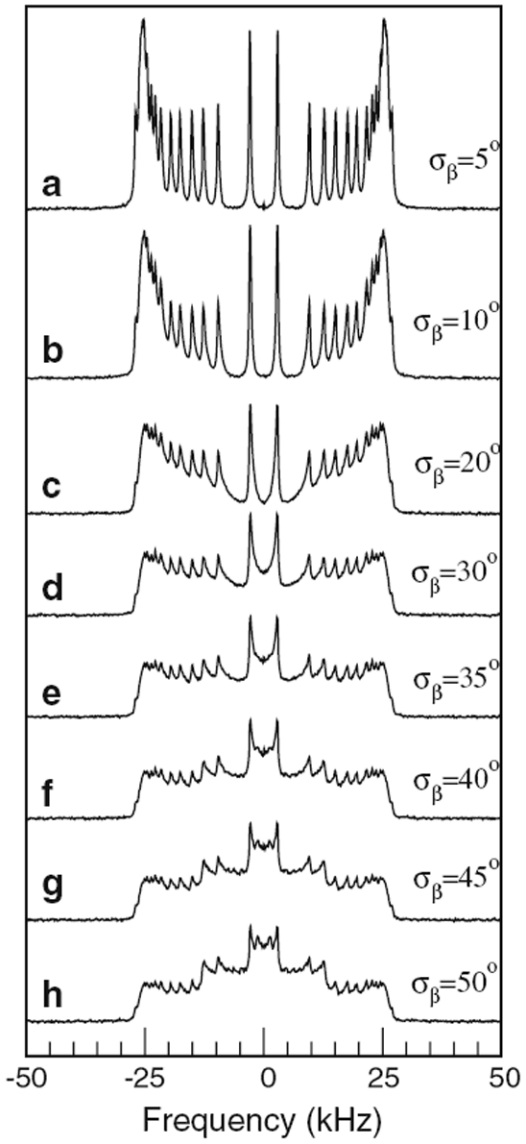

Fig. 4.

Simulations of oriented POPC-d_{31} bilayers with mosaic spread modeled by a Gaussian distribution of bilayer normal orientations with distribution widths of *a* $\sigma_\beta = 5°$, *b* $\sigma_\beta = 10°$, *c* $\sigma_\beta = 20°$, *d* $\sigma_\beta = 30°$, *e* $\sigma_\beta = 35°$, *f* $\sigma_\beta = 40°$, *g* $\sigma_\beta = 45°$, and *h* $\sigma_\beta = 50°$. Order parameters were taken from the order parameter profile of the peptide-free vesicle sample in Fig. 1g. Line width was adjusted such that, in the absence of mosaic spread, it approximated that of oriented POPC-d_{31}/POPG

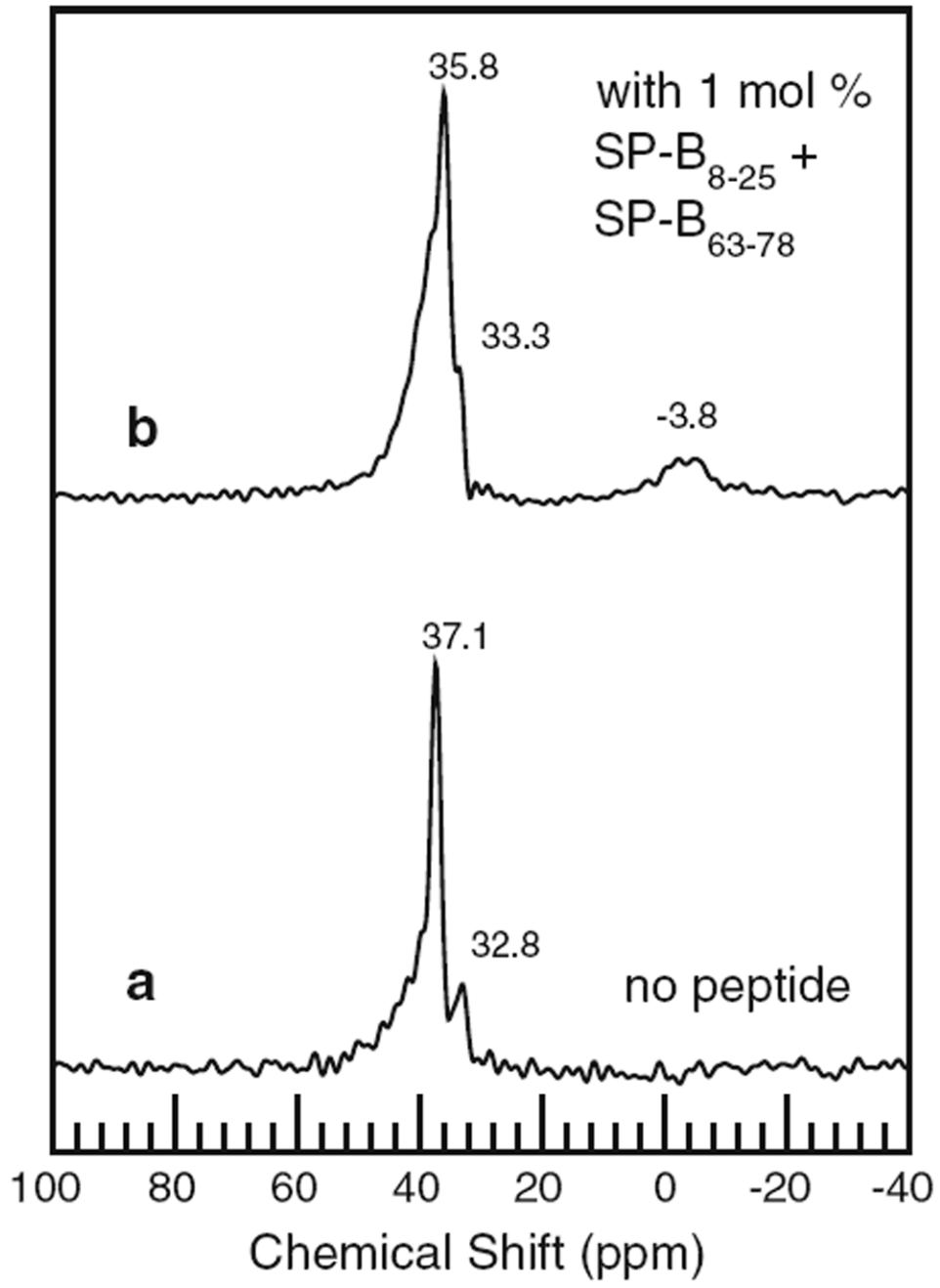

Fig. 5.

^{31}P NMR spectra of mechanically oriented bilayer samples containing POPC-d_{31}/POPG (7:3) with no peptide (*a*) and 1 mol% SP-$B_{8–25}$ and SP-$B_{63–78}$ peptide separately (*b*). All data taken at 23 °C

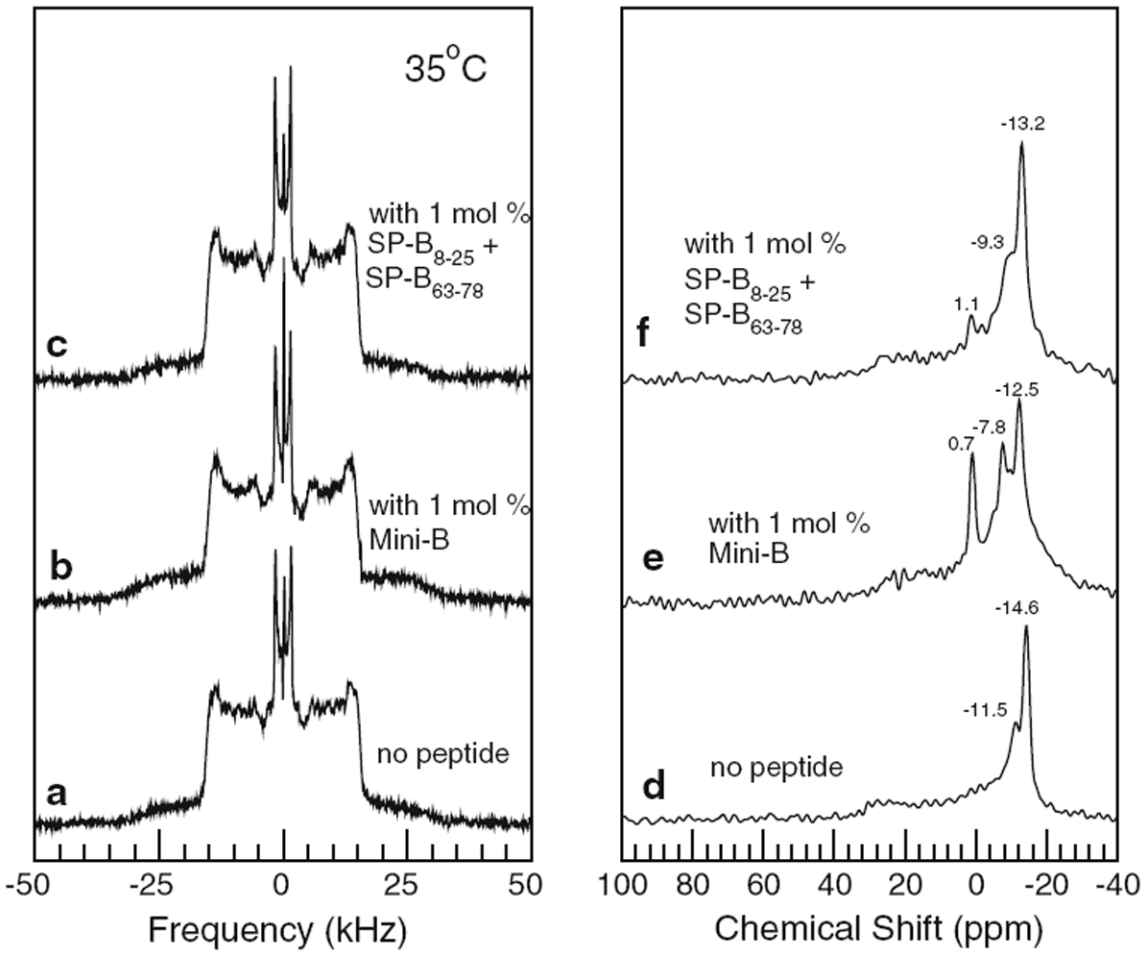

Fig. 6.

Left panel ^{2}H NMR spectra of multilamellar vesicle dispersions of bovine lipid extract surfactant (BLES) doped with DPPC-d_{62} (2.5 % w/w) containing no peptide (*a*), 1 mol% Mini-B (*b*), and 1 mol% SP-$B_{8–25}$ and SP-$B_{63–78}$ peptide separately (*c*). *Right panel* Corresponding ^{31}P NMR spectra of multilamellar vesicle dispersions of bovine lipid extract surfactant (BLES) doped with DPPC-d_{62} (2.5 % w/w) containing no peptide (*d*), 1 mol% Mini-B (*e*), and 1 mol% SP-$B_{8–25}$ and SP-$B_{63–78}$ peptide separately (*f*). All data taken at 35 °C

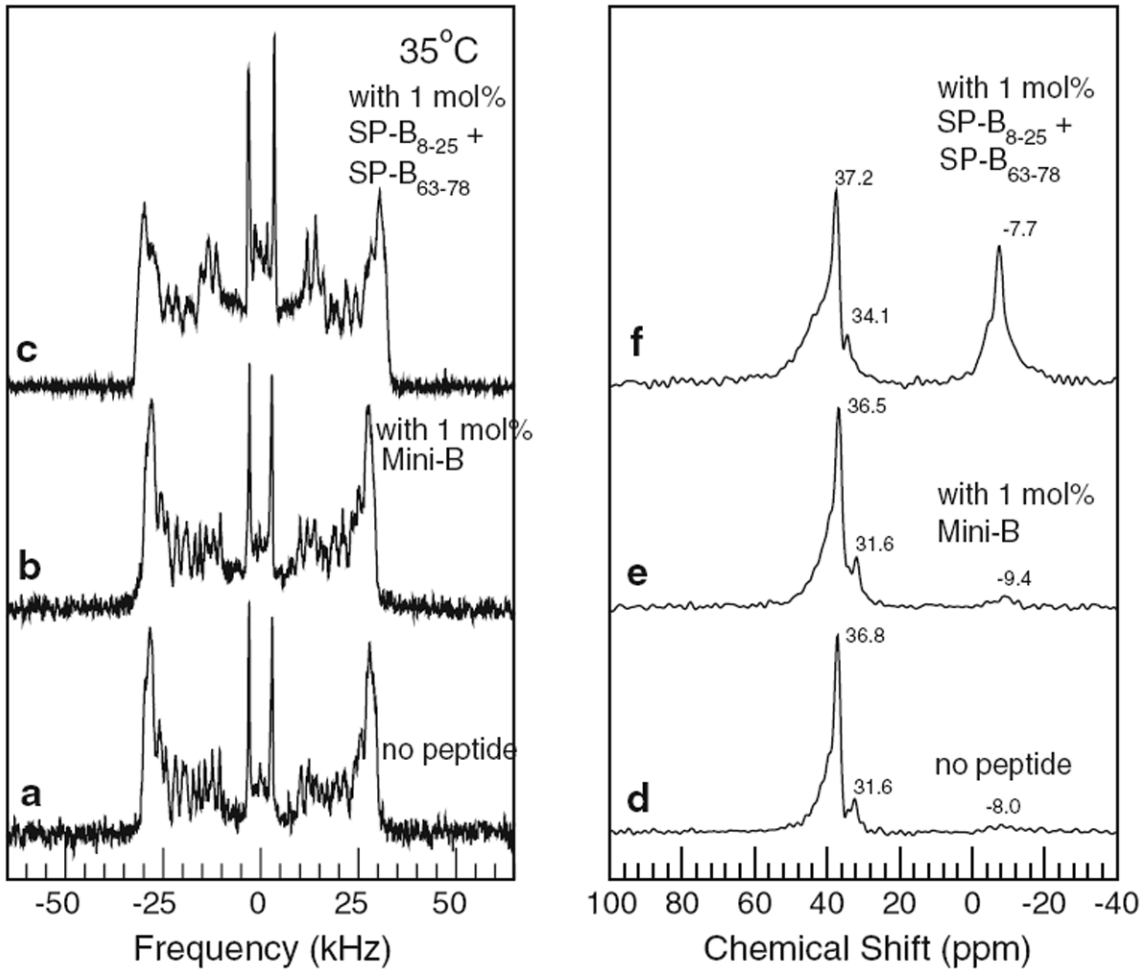

Fig. 7.

Left panel ^{2}H NMR spectra of mechanically oriented bilayers of bovine lipid extract surfactant (BLES) doped with DPPC-d_{62} (2.5 % w/w) containing no peptide (*a*), 1 mol% Mini-B (*b*), and 1 mol% SP-$B_{8–25}$ and SP-$B_{63–78}$ peptide separately (*c*). *Right panel* Corresponding ^{31}P NMR spectra of mechanically oriented bilayers of bovine lipid extract surfactant (BLES) doped with DPPC-d_{62} (2.5 % w/w) containing no peptide (*d*), 1 mol% Mini-B (*e*), and 1 mol% SP-$B_{8–25}$ and SP-$B_{63–78}$ peptide separately (*f*). All data taken at 35 °C